Robust Neural Controllers for Power System Based on New Reduced Models

Wissem BAHLOUL[1], *Mohamed CHTOUROU*[2], *Mohsen BEN AMMAR*[2], *Hsan HADJABDALLAH*[2]

[1]Biomedical Department, Higher Institute of Biotechnology of Sfax, University of Sfax, Street Soukra, 3029 Sfax, Tunisia
[2]Department of Electrical Engineering, National Engineering School of Sfax, University of Sfax, Street Soukra, 3029 Sfax, Tunisia

wissem.bahloul@isbs.usf.tn, mohamed.chtourou@enis.rnu.tn, mohsen.benammar@enis.tn, hsan.haj@enis.rnu.tn

DOI: 10.15598/aeee.v21i2.4690

Article history: Received Sep 01, 2022; Revised Jan 14, 2023; Accepted Mar 27, 2023; Published Jun 30, 2023.

Abstract. *This paper presents an advanced control method for the stabilization of Electric power systems. This method is a decentralized control strategy based on a set of neural controllers. Essentially, the large-scale power system is decomposed into a set of subsystems in which each one is constituted by a single machine connected to a variable bus. For each subsystem, a neural controller is designed to respond to a performance index. The neural controller is a feed-forward multi-layered one. Its training method is accomplished for different rates of desired terminal voltage and is based on the perturbed electrical power system model. For a single machine, the synaptic weights of corresponding neural controller are adjusted to force the machine outputs to converge into expected one obtained by the load flow program. To evaluate the performance and effectiveness of the proposed control method, it has been applied to the WSCC power system under severe operating conditions. The obtained results compared to the ones of conventional controllers proved the high quality of the proposed controller in terms of transient stability and voltage regulation of the considered electrical power system.*

Keywords

Decentralized control, mathematic model reduction, neural controller, power system.

1. Introduction

To maintain the interconnected power system stability under several disturbances, robust excitation controllers are used for the different generators [1] and [2]. These controllers require the entire power system state variables to be available at one central computing station in order to make centralized controller law [3] and [4]. However, several researchers have pointed out that the implementation of a centralized controller possesses certain difficulties, particularly when the complexity of the interconnected area increases [5], [6], [7] and [8]. More importantly, the centralized control poses a heavy risk of instability if a loss or retard of information occurs in their communication system. In this respect, a decentralized control approach is used [9], [10], [11], [12], [13], [14], [15], [16], [17] and [18]. The advantage of the decentralized control applications does reduce the complexity of the system model and allows more feasible control implementation. Several design approaches have been proposed and successfully applied to improve the transient power system stability. In [9], based on the LMI approach, a decentralized controller is designed. In [10], a $H\infty$ controller for Single Machine Infinite Bus (SMIB) system is proposed. A decentralized controller is designed for a varying system model as presented in [11]. However, most of these works just employ the linearized power system model for designing these controllers. Generally, the SMIB system is simplified and linearized as a single machine connected to an infinite bus model under normal operating conditions. It is obvious that

when major or inter-zone faults occur, the behaviour of the power system may change significantly. Therefore, the conventional linear controllers are not sufficient to guarantee the system stability under these circumstances.

In recent years, in order to improve the transient stability, much more attention has been paid to power system control, using the latest developed nonlinear control theory [19], [20] and [21]. Taking the other view into consideration, the modelling of the whole Electric Power System (EPS) for the decentralized control represents a challenge for many recent researchers [22], [23], [24] and [25]. In order to enhance the stability of the interconnected nonlinear power systems within the whole operating region, the design of the decentralized nonlinear controllers still remains a challenging task for researchers in this area of study. Different techniques of nonlinear controller are proposed in the literature and the learning capacities of the nonlinear neural controller [26], [27], [28], [29] and [30] for a system with complex nonlinear behaviour as well as for an extended domain of operation is a potential solution for designing a new controller.

Accordingly, a neural control, which is proposed by some researchers in the last 40 years has been continuously evolving until today. In 1990 [26], Nguyen and Widrow introduced a new schema of neural control with a full state feedback and an emulator for designing a dynamic system. The backpropagation algorithm and the specialized training method are operated in this paper. However, authors in [27] suggested another schema of neural control with output feedback. They investigated two types of training methods; generalized and specialized. Jadlovsa published a paper in 2000 [28] that focuses on the control structure for target and trajectory tracking by neuro-controller, which drives a dynamical system from an initial condition to given finite states. In some other papers [29], [30], [31], [32] and [33], a novel intelligent system with adaptive control architecture for power system is designed. It mainly contains two neural networks: one as a controller and another as an identifier. The last system is trained with extensive test data offline in addition to an adjusted online one.

In the current investigation, a new robust decentralized neural controller is proposed and developed, which uses only local information for a large interconnected nonlinear power system. Accordingly, two stages are actually to pursue: in the first, the whole interconnected power system is decomposed into independent sub-systems founded on load flow program results and new reduction method. Then, the multi-machine power system model is transformed into independent reduced models designed for each generator separately. Each model consists of a single generator connected to a variable Bus. The last Bus is designed by three new parameters (R_i, X_i and V_{si}). By adapting the parameters values in the healthy and faulty system states, the proposed independent dynamic model for each generator makes it possible to design three topologies for each sub-system states (before fault, during fault and after fault). In the second stage, each sub-system designed with reduced model is controlled using Decentralized Neural Controller (DNC) techniques. The considered neural controller has been nominated as robust one because it has been trained for different fault types occurring in the power system. For these different faults, different mathematical models representing the faulted multi-machine power system have been considered for the training of the neural controller. Seizing the performances of the neural controller offered by authors in [27], the terminal voltage of each generating buses is oriented to this aimed value. For the training of the DNC, the specialized learning architecture is used to specifically learn in the region of interest. In this case, no stability problems for the control system are noticed [26] and [27].

This paper is structurally written as follows. Section 2. details the reduction method of the EPS. The DNC design is introduced in Sec. 3. In order to validate the proposed controller, simulation results are provided in Sec. 4. Lastly, the conclusion is given in Sec. 5.

2. Reduction Method of the Interconnected Power System Model

The fame multi-machine model of interconnected power system is complex and multivariable [1] and [2]. A new reduction method is proposed in order to synthesize a robust decentralized neural controller consisting in simplifying the complexity of the model and reducing the number of numerous variables.

2.1. Aggregation of the Power System Producer Nodes

The EPS is designed for n nodes, which are classified into two types: the nodes producing N_g numbers and the others consuming N_c Numbers. It is worth noticing that the nodes total number is equal to $N = N_g + N_c$. The expression of the injected current $\bar{I}_i$ in each node of the power system is expressed by the following expression:

$$\bar{I}_i = \sum_{j=1}^{N} \bar{Y}_{Nij} \bar{V}_j. \tag{1}$$

Thus, the matrix writing of the current is given by:

$$\bar{I} = \bar{Y}_N \bar{V}, \tag{2}$$

where $\bar{Y}_N$ denotes the nodal matrix of dimension $(N \times N)$. By decomposing the vector $\bar{I}$ into two sub-ones, each is corresponding to the currents injected in the load nodes and to the number N_c. The currents injected in the generator nodes correspond to the number N_g. Accordingly, the matrices $\bar{Y}_N$ and $\bar{V}$ will be decomposed by the same manner. In this respect, the last matrix Eq. (2) turns up into the following form:

$$\bar{I} = \begin{bmatrix} -\bar{I}_{cc} \\ \cdots\cdots\cdots\cdots \\ \bar{I}_g - \bar{I}_{cp} \end{bmatrix} = \begin{bmatrix} \bar{Y}_{cc} & \vdots & \bar{Y}_{cp} \\ \cdots\cdots\cdots\cdots & & \cdots\cdots \\ \bar{Y}_{cp}^T & \vdots & \bar{Y}_{pp} \end{bmatrix} \begin{bmatrix} \bar{V}_c \\ \cdots\cdots \\ \bar{Y}_p \end{bmatrix} \begin{matrix} \downarrow & N_c \\ - & - \\ \uparrow & N_g \end{matrix}. \tag{3}$$

The load current is expressed as a function of bus voltage $\bar{Y}_i$, real and reactive power (P_{ci} and Q_{ci}) obtained by Load Flow Program (LFP):

$$\bar{I}_{ci} = \bar{Y}_{ci} \bar{V}_i, \tag{4}$$

where $\bar{Y}_{ci} = \dfrac{P_{ci} + jQ_{ci}}{V_i^2}$.

Thus, the last current can be written in the following matrix form:

$$\bar{I}_c = \bar{Y}_c \bar{V}. \tag{5}$$

Similarly to the above decomposition, the vectors $\bar{I}_c$ is expressed as follows:

$$\bar{I}_c = \begin{bmatrix} \bar{I}_{cc} \\ \cdots\cdots\cdots \\ \bar{I}_{cp} \end{bmatrix} = \begin{bmatrix} \bar{Y}_c & \vdots & 0 \\ \cdots\cdots\cdots\cdots & & \cdots\cdots \\ 0 & \vdots & \bar{Y}_p \end{bmatrix} \cdot \begin{bmatrix} \bar{V}_c \\ \cdots\cdots \\ \bar{Y}_t \end{bmatrix}, \tag{6}$$

where the sub-vectors $\bar{V}_c$ and $\bar{V}_t$ define the voltages at the consuming nodes and at the terminals of the generators connected to the EPS, respectively. Indeed, the sum of the two vectors of the injected currents $\bar{I}$ given by Eq. (3) and the load current $\bar{I}_c$ given by Eq. (6) provides the following Eq. (7):

$$\begin{bmatrix} 0 \\ \cdots\cdots \\ \bar{I}_g \end{bmatrix} = \begin{bmatrix} \bar{Y}_{cc} & \vdots & \bar{Y}_{cp} \\ \cdots\cdots\cdots\cdots & & \cdots\cdots \\ \bar{Y}_{cp}^T & \vdots & \bar{Y}_{pp} \end{bmatrix} \cdot \begin{bmatrix} \bar{V}_c \\ \cdots\cdots \\ \bar{Y}_t \end{bmatrix}, \tag{7}$$

which makes it possible to express the generator nodes current vector $\bar{I}_g$ by the following matrix equation:

$$\bar{I}_g = \bar{Y}_p \bar{V}_t, \tag{8}$$

where $\bar{Y}_p = \left[\bar{Y}'_{pp} - \bar{Y}_{cp}^T(-\bar{Y}'_{cc})^{-1}\bar{Y}_{cp}\right]$, which is the reduced admittance matrix. Its dimension has been reduced from $(N \times N)$ to $(N_g \times N_g)$. This procedure, therefore, is helpful to switch from a grid of $N = N_g + N_c$ nodes to another reduced one of N_g producer nodes. Hence, the interconnected power system aggregated by the N_g producer nodes is schematized in Fig. 1.

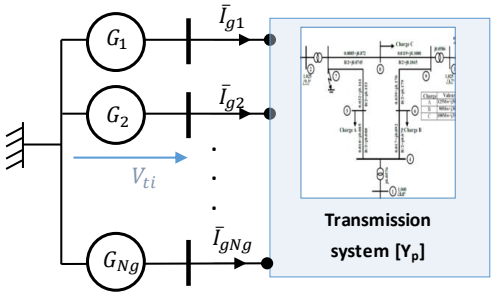

Fig. 1: The interconnected power system aggregated by the N_g producer nodes.

2.2. Decoupling of Each Generator as Single Machine Sub-system

For decoupling each generator in independent sub-system, the matrix expression (Eq. (8)) can be inverted to formulate the vector of the voltages at the generating nodes:

$$\bar{V}_t = \bar{Z}_p \bar{I}_g, \tag{9}$$

where $\bar{Z}_p = \bar{Y}_p^{-1}$. Based on Eq. (9), the terminal voltage of the i$^{\text{th}}$ node generator can be transformed regarding impedances and injected currents by:

$$\bar{V}_{ti} = \sum_{j=1}^{N_g} \bar{Z}_{ij}\bar{I}_{gj} = \bar{Z}_{ii}\bar{I}_{gi} + \sum_{\substack{j=1 \\ j\neq i}}^{N_g} \bar{Z}_{ij}\bar{I}_{gj}. \tag{10}$$

The injected current of each generator node $\bar{I}_{gj}$ considering the equation is possibly expressed as follows:

$$\bar{I}_{gj} = \sum_{k=1}^{Ng} \bar{Y}_{jk}\bar{V}_{tk}. \tag{11}$$

Replacing the expression $\bar{I}_{gj}$ in Eq. (10), the terminal voltage of the ith node generator is obtained by:

$$\bar{V}_{ti} = \bar{Z}_{ii}\bar{I}_{gi} + \sum_{\substack{j=1\\ j\neq i}}^{N_g} \bar{Z}_{ij} \sum_{k=1}^{N_g} \bar{Y}_{jk}\bar{V}_{tk} =$$

$$= \bar{Z}_{ii}\bar{I}_{gi} + \sum_{\substack{j=1\\ j\neq i}}^{N_g} \bar{Z}_{ij} \sum_{\substack{k=1\\ k\neq i}}^{N_g} \bar{Y}_{jk}\bar{V}_{tk} + \bar{V}_{ti} \sum_{\substack{j\neq=1\\ j\neq i}}^{N_g} \bar{Z}_{ij}\bar{Y}_{ji}, \tag{12}$$

$$\bar{V}_{ti}\left(1 - N_g \bar{Z}_{ij}\bar{Y}_{ji}\right) = \bar{Z}_{ii}\bar{I}_{gi} + \sum_{\substack{j=1\\ j\neq i}}^{N_g} \bar{Z}_{ij} \sum_{\substack{k=1\\ k\neq i}}^{N_g} \bar{Y}_{jk}\bar{V}_{tk}, \tag{13}$$

we pose: $\mu_i = \dfrac{1}{1 - \sum\limits_{\substack{j=1\\ j\neq i}}^{N_g} \bar{z}_{ij}\bar{\gamma}_{ji}}$,

then $\bar{V}_{ti} = \mu_i \bar{Z}_{ii}\bar{I}_{gi} + \mu_i \sum\limits_{\substack{j=1\\ j\neq i}}^{N_g} \bar{Z}_{ij} \sum\limits_{\substack{k=1\\ k\neq i}}^{N_g} \bar{Y}_{jk}\bar{V}_{tk}$.

Basing on Eq. (12) and Eq. (13), the i$^{\text{th}}$ generator node terminal voltage is solely represented with an equivalent impedance and voltage, as follow:

$$\bar{V}_{ti} = \bar{Z}_i\bar{I}_{gi} + \bar{V}_{si}, \tag{14}$$

with: $\bar{V}_{si} = \mu_i \sum\limits_{\substack{j=1\\ j\neq i}}^{N_g} \bar{Z}_{ij} \sum\limits_{\substack{k=1\\ k\neq i}}^{N_g} \bar{Y}_{jk}\bar{V}_{tk}$. In the same context, we pose:

$$V_s i = |\bar{V}_s i|, \tag{15}$$

$$R_i = real(\bar{R}_i), \tag{16}$$

$$X_i = Imag(\bar{Z}_i). \tag{17}$$

Consequently, using Eq. (14) allows us to model the power system as an independent N_g generator connected to the rest of the grid. Hence, the rest of the EPS is assimilated by an impedance $\bar{Z}_i$ in series with a voltage source $\bar{V}_{si}$ as shown in Fig. 2 which represents new mathematic reduction model for power system. The parameters rates (R_i, X_i and V_{si}) for any steady state are calculated by Eq. (15), Eq. (16) and Eq. (17): this means that each generator has an aggregate view of the remaining $N_g - 1$ generators equivalent to *a variable parameter bus* (see Fig. 2).

For the *study and control of the transient regime*, the generator G_i will be modeled by its adequate dynamic model.

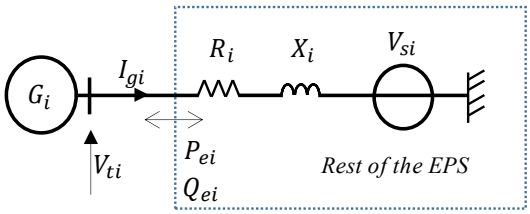

Fig. 2: Reduced model for power system used for decoupling of the i$^{\text{th}}$ generator.

2.3. Dynamic Model of Synchronous Generator

The detailed nonlinear model of a synchronous generator is a seventh-order model while the popular third-order model is of crucial interest for studying control systems of the generator as well as their stability analysis [1] and [2]. Therefore, the detailed nonlinear model is usually reduced to a generalized nonlinear third-order model [1]. It is expressed per unit as follows:

$$\begin{cases} \frac{d\delta i(t)}{dt} = \omega_i(t), \\ \frac{d\omega i(t)}{dt} = -\frac{K_{Di}}{2H_i}\omega_i(t) + \frac{\omega_s}{2H_I}\left(P_{mi}(t) - P_{ei}(t)\right), \\ \frac{dE'_{qi}(t)}{dt} = \frac{1}{T'_{d0i}(t)}\left(E_{fdi}(t) - \left(E'_{qi} + (X_{di} - X'_{di})\, I_{di}\right)\right), \end{cases} \tag{18}$$

where δ_i is the generator rotor angle, ω_i is the difference between the generator angular speed and the synchronous angular speed, E'_{qi} is the transient EMF in quadrature axis q and P_{ei} is the electrical power. P_{mi} and E_{fdi} are the two inputs of the system corresponding to the mechanical power and the excitation control voltage, respectively. K_{Di}, H_i and T'_{d0i} are the dumping constant, the inertia constant and the excitation circuit time constant, respectively.

The Blondel diagram corresponding to the synchronous generator using to calculate the algebraic electrical equations is presented by Fig. 3 [1]. In this diagram, the terminal voltage of the ith generator is expressed by the sum vector: $\bar{V}_t i = \bar{V}_{si} + R_i\bar{I}_{gi} + jX_i\bar{I}_{gi}$.

Referring to the Blondel diagram, the algebraic electrical equations could be calculated as:

$$P_{ei} = E_{qi}I_{qi}, \tag{19}$$

$$E_{qi} = E'_{qi} + \Delta X_{di}I_{di}, \tag{20}$$

$$I_{di} = \frac{\left(X_{qsi}E'_{qi} - (X_{qsi}V_{qi} + R_iV_{di})\right)}{R'_{xi}}, \tag{21}$$

$$I_{qi} = \frac{\left(R_iE'_{qi} + X_d si' V_{di} - R_iV_{qi})\right)}{R'_{xi}}, \tag{22}$$

where $V_{qi} = V_{si}\cos(\delta_i)$; $V_{di} = V_{si}\sin(\delta_i)$; $X'_{dsi} = X'_{di} + X_i$; $X_{dsi} = X_{di} + X_i$; $X_{qsi} = X_{qi} + X_i$; $R_x i' = R_i^2 + X'_{dsi}X_{qsi}$; $R_x i = R_i^2 + X_{dsi}X_{qsi}$ and $\Delta X_{di} = X_{di} - X'_{di}$.

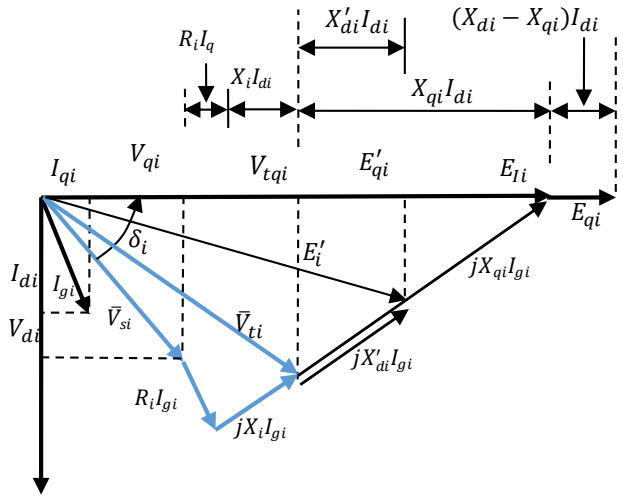

Fig. 3: Blondel diagram of one machine connected to the power system.

By referring to Eq. (19), Eq. (20), Eq. (21) and Eq. (22) and by exploiting the coefficients a_{ji} given in Tab. 1, the electric power expression is given by:

$$P_{ei}(t) = (a_{1i}\cos(\delta_i) + a_{2i}\sin(\delta_i) + a_{3i}E'_{qi})E'_{qi} + \\ + a_{4i}\sin^2(\delta_i) + a_{5i}sin(2\delta_i) + a_{0i}. \tag{23}$$

Tab. 1: Coefficients of electrical power equation.

Coefficients	Quantity
a_{0i}	$\frac{R_iX_{qs}WiV_{si}^2\Delta X_{di}}{R_x'^2}$
a_{1i}	$\frac{-R_iV_{si}(R_{xi}+X_qsi\Delta X_{di})}{R_{xi}'^2}$
a_{2i}	$\frac{V_{si}(R_{xi}X_dsi' - R_i^2\Delta X_{di})}{R_{xi}'^2}$
a_{3i}	$\frac{R_iR_x}{R_x'^2}$
a_{4i}	$\frac{-R_i\Delta X_{di}V_{si}^2(X_qsi+X_dsi')}{R_i}$
a_{5i}	$\frac{\Delta X_{di}V_{si}^2(R_i^2 - X_dsi'X_qsi)}{2R_{xi}'^2}$

Replacing P_{ei} and I_{di} by their expressions, the dynamic model of the synchronous machine connected to the rest of the grid is given by the state model presented by Eq. (24):

$$\begin{cases} \frac{d\delta_i}{dt} = \omega_i, \\ \frac{d\omega_i}{dt} = -\frac{K_{Di}}{2H_i}\omega - \frac{\omega_s}{2H_i}\left[P_{mi} + a_{0i} + E'_{qi}\left(a_{1i}\cos\delta_i + \right.\right. \\ \left. + a_{2i}\sin\delta_i + a_{3i}E'_{qi}\right) + a_{4i}\sin^2\delta_i + a_{5i}\sin 2\delta_i\Big], \\ \frac{dE'_{qi}}{dt} = \frac{1}{T'_{d0i}}\left(a_{6i}E'_{qi} + a_{7i}\sin\delta_i + a_{8i}\cos\delta_i + E_{fdi}\right), \end{cases} \tag{24}$$

where $a_{6i} = \frac{-R_{xi}}{R'_{xi}}$; $a_{7i} = \frac{R_iV_{si}}{R'_{xi}}\Delta X_{di}$ and $a_{8i} = \frac{X_{qsi}V_{si}}{R'_{xi}}\Delta X_{di}$.

From another perspective, the generator terminal voltage V_{ti} represents the measurable output of the generator. According to Blondel's diagram, the direct and quadrature components of V_{ti} are illustrated by:

$$V_{tdi} = -X_{qi}I_{qi}, \tag{25}$$

$$V_{tqi} = E'_{qi} - X'_{di}I_{di}, \tag{26}$$

$$V_{ti} = \sqrt{V_{tdi}^2 + V_{tqi}^2}. \tag{27}$$

By replacing I_{di} and I_{qi} by their expressions in Eq. (21) and Eq. (22), we obtain the new expression for the generator terminal voltage:

$$V_{ti}(t) = \frac{1}{R'_{xi}}\left(b_{0i} + E'_{qi}\left(b_{1i}\sin\delta_i + b_{2i}\cos\delta_i + b_{3i}E'_{qi}\right) + \right. \\ \left. + b_{4i}\sin^2\delta_i + b_{5i}\sin 2\delta_i\right)^{0.5}, \tag{28}$$

where the coefficients b_{ji} are given in Tab. 2 below.

Tab. 2: Coefficients of terminal voltage equation.

Coefficients	Quantity
b_{0i}	$V_{si}^2(R_i^2X_{qi}^2 + X_{qsi}^2X_{di}'^2)$
b_{1i}	$2V_{si}R_i(X'_{dsi}X_{qi}^2 - X_{di}'^2X_{qsi} + R'_{xi}X'_{di})$
b_{2i}	$2V_{si}(R'_{xi}X'_{di}X_{qsi} - R_i^2X_{qi}^2 - X_{qsi}^2X_{di}'^2)$
b_{3i}	$R_{xi}'^2 + (R_i^2X_{qi}^2 + X_{qsi}^2X_{di}'^2 - 2R'_{xi}X'_{di}X_{qsi})$
b_{4i}	$V_{si}^2(X_{qi}^2X_{dsi}'^2 + R_i^2(X_{di}'^2 - X_{qi}^2) + X_{qsi}^2X_{di}'^2)$
b_{5i}	$V_{si}^2R_i(X_{di}'^2X_{qsi} - X'_{dsi}X_{qi}^2)$

The quantities available to act on the behavior of the power system are the mechanical input power applied to the machine shaft and the rotor excitation signal. In this design, we assume that the mechanical input power P_{mi} is slowly changing compared to the excitation control voltage. Thus, let $P_{mi} = P_{mi0}$ be a positive constant and the only control input signal is $u(t) = E_{fdi}(t)$.

The state space model of the power system presented by Eq. (24) has a nonlinear behavior, which can be given by:

$$\begin{cases} \dot{X} = A(X(t),\theta(t))\cdot X(t) + B\cdot u(t), \\ Y(t) = h(X(t),\theta(t)), \end{cases} \tag{29}$$

where $X(t) \in \mathbb{R}^3$ denotes the vectors of the 3 states, $Y(t) \in \mathbb{R}^2$ is column that represents the 2 outputs and $\theta(t)$ represents vector

variable parameters: $X(t) = [\delta_i(t)\omega_i(t)E'_{qi}(t)]^T$, $Y(t) = [\omega_i(t)V_{ti}(t)]^T$, $\theta(t) = [R_i(t)X_i(t)V_{si}(t)]^T$,

$$A = \begin{bmatrix} 0 & 1 \\ \frac{\omega_s}{2H_i\delta_i}\begin{pmatrix} a_{4i}\sin^2\delta_i + \\ a_{5i}\sin 2\delta_i \end{pmatrix} & -\frac{K_{Di}}{2H_i} \\ \frac{1}{T'_{d0i}\delta_i}\begin{pmatrix} a_{7i}\sin\delta_i + \\ a_{8i}\cos\delta_i \end{pmatrix} & 0 \end{bmatrix}$$

$$\begin{bmatrix} 0 \\ \frac{\omega_s}{2H_i}\begin{pmatrix} a_{1i}\cos\delta_i + \\ a_{2i}\sin\delta_i + a_{3i}E'_{qi} \end{pmatrix} \\ \frac{a_{6i}}{T'_{d0i}} \end{bmatrix},$$

$$B = \begin{bmatrix} 0 & 0 \\ \frac{P_m + a_0}{2H_i} & 0 \\ 0 & \frac{1}{T'_{d0i}} \end{bmatrix}, \begin{bmatrix} 0 \\ E_{fd}(t) \end{bmatrix}$$ and h represents the observation equation: $h = [\omega_i(t)V_{ti}(t)]^T$.

In this study, the machine model has been used in its discrete form according to Euler's method with a sampling time T_e:

$$\begin{cases} X(k+1) = (I + T_e \cdot A)\, X(k) + T_e \cdot B \cdot U, \\ Y(k) = h(X(k), \theta(k)). \end{cases} \quad (30)$$

3. Proposed Decentralized Neural Control Strategy

Besides, the nonlinearity and the complexity of the model above (Eq. (30)), the EPS can be the site of different default types in disturbance states. For this reason and exploiting the neural networks capacity of learning different functioning conditions, a neural control will be considered for the excitation command of the generators connected to the EPS. The neural control strategy inspired by [27] have shown noticeable performances and use only outputs as feedback signal.

3.1. The Neural Control Scheme

The neural control scheme consists in associating a Neural Controller (NCi) with each machine, which maintains its terminal voltage round a desired one and mainly to enhance the transient stability even in the presence of severe perturbations in the EPS. For *illustrative reasons*, the suggested control structure for an EPS composed by three generators ($N_g = 3$) is presented by Fig. 4.

The suggested control strategy is a decentralized one where a decentralized neural controller is trained for each single machine and different operating conditions. Two types of faults are considered: local and inter-zone one. Strategy requires only direct measurements from individual generators, thereby making implementation simple in practice.

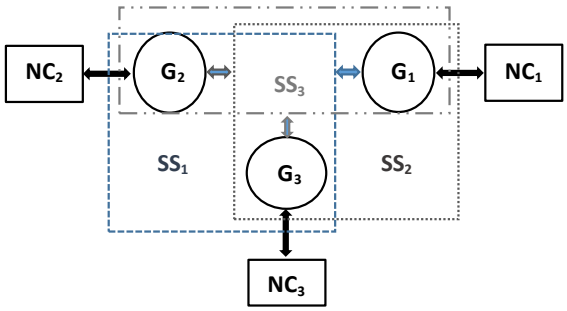

Fig. 4: The control structure scheme corresponding to each generator of the EPS.

3.2. Synthesis of the Neural Controllers

In this section, the synthesis of the neural controller associated with each machine will be deeply analyzed. It is a feed forward multilayered network. Its input is constituted by the desired value of the terminal voltage at future instant $(k+1)$, the actual terminal voltage and generator deviation speed. The output of the neural controller is the actual excitation voltage to be applied for the machine (see Fig. 5).

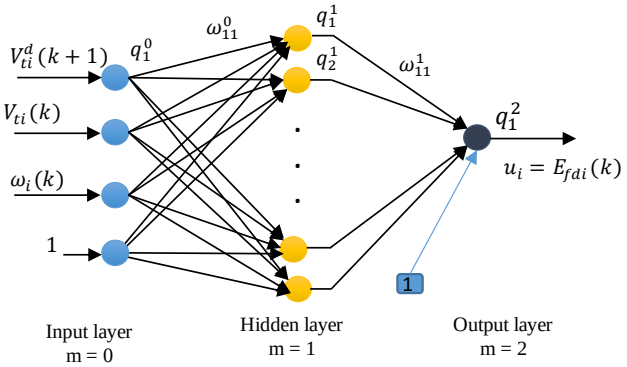

Fig. 5: The three conditions steady state: before, during and after fault.

1) Neural Controller Architecture

The neural controller is composed of one hidden layer and one output neuron. The numbers of hidden neurons will be fixed following learning trials. In this case, the architecture, which delivers the minimum error, is chosen. Furthermore, the most used activation function for hidden layer is that of sigmoid and for input and output layer is the linear one. The suggested $\frac{1}{2}$ architecture of the neural controller is given by Fig. 5.

Referring to this architecture of the NC, the outputs of the neuron (a) at layer (m) are done by the following expression:

$$q_a^m = f_a^m(\sum_b \omega_{ab}^m q_b^{m-1}), \tag{31}$$

where f_a^m are the activation functions.

2) Training Method

In order to train an efficient neural controller, different types of eventual faults have been considered, local and inter-zone one [1]. Essentially, the equivalent circuit is specified by three different steps: before a fault, during the fault and after the elimination of the fault. It is worth noting that the values of the new parameters (R_i, X_i and V_{si}) are variable and *the faulted grid is considered in the steady state.*

For each steady state, the values of the new parameters are computed by *a load flow program and reduction equations* (Eq. (15), Eq. (16) and Eq. (17)) and then, updated in the single machine dynamic model which will be used in the training algorithm.

The neural controller training has been accomplished based on the Fig. 6 which can be considered as a specialized training strategy [27]. The NCi is trained to find the actual SSi input $u(k)$ that drives the system outputs Y to the desired Y^d. This is accomplished by using the error between the desired and system outputs at future instant $(k+1)$ to adjust the weights of the network using a descent procedure.

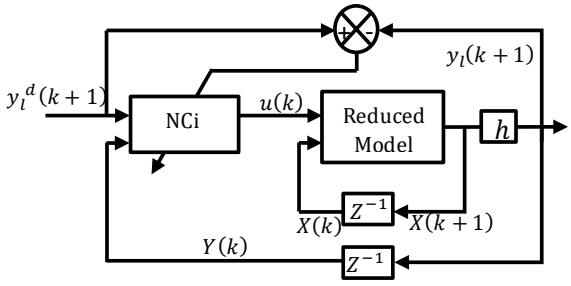

Fig. 6: The training process of the neural network controller.

The weights of each NCi are updated to minimize the mean-square error.

$$J(k) = \frac{1}{2}\sum_{l=1}^{2} \alpha_l (y_l^d(k+1) - y_l(k+1))^2, \tag{32}$$

where the constants α_l are chosen by the designer to weigh the importance of each output error component in the control process. The final desired responses are: $y_1^d = 0$ and $y_2^d = V_t^d$, where $y_l(k+1)$ denotes the predicted outputs as functions of future states $X(k+1)$ and the input at time instant k.

Taking each distinctive iterative process into consideration, the neural controller weights are adjusted using gradient method:

$$\omega_{ab_{new}}^m = \omega_{ab_{old}}^m - \gamma \frac{\partial J(k)}{\partial \omega_{ab}^m}, \tag{33}$$

where the learning rate value γ is chosen in order to fix the convergence speed of the training algorithm.

$$\frac{\partial J(k)}{\partial \omega_{ab}^m} = \delta_{ab}^m \sum_{l=1}^{2} \left(y_l^d(k+1) - y_l(k+1)\right) \frac{\partial y_l(k+1)}{\partial u(k)}, \tag{34}$$

where δ_{ab}^m are obtained from Eq. (31) of NCi:

$$\delta_{a1}^1 = \frac{\partial u(k)}{\partial \omega_{a1}^1} = u(k)(1-u(k))q_a^1, \tag{35}$$

$$\delta_{ab}^0 = \frac{\partial u(k)}{\partial \omega_{ab}^0} = u(k)(1-u(k))\omega_{a1}^1 q_b^1 \left(1-q_b^1\right) q_a^0. \tag{36}$$

To determine the derivative of the SS_i, outputs at future instant $y_l(k+1)$ with respect to his actual input $u(k)$ are obtained by using the Jacobian of discrete model Eq. (30):

$$\frac{\partial y_1(k+1)}{\partial u(k)} = T_e^2 k_{11i}\omega_s \left[k_{2i}\cos\left(x_1(k)\right) + \right. \\ \left. + k_{3i}\sin\left(x_1(k)\right) + 2k_{4i}x_3(k)\right], \tag{37}$$

$$\frac{\partial y_2(k+1)}{\partial u(k)} = \frac{1}{2} y_2(k) T_e k_{11i} \left(C_{2i}\sin\left(x_1(k)\right) + \right. \\ \left. + C_{3i}\cos\left(x_1(k)\right) + 2C_{4i}x_3(k)\right). \tag{38}$$

4. Validation of the DNC

The WSCC system [34] shown in Fig. 7 is used as an exemplar system to test the performance of the proposed decentralized neural controllers.

As it is presented in Fig. 4, each neural controller $NC_i (i = 1, 2, 3)$ is applied to each corresponding generator G_i at the same time. Within a simulated process, the proposed robust neural excitation controller is compared to linear AVR+PSS excitation one [35]. Accordingly, several sequences are studied in order to show the effectiveness of the proposed nonlinear control. Indeed, a rich database was used for the learning phase of the NC.

4.1. Learning Phase

Learning is carried out for *three faulted states characterized* by: a step change in load at the consumer nodes (node 2, 3 and 5), a three-phase short-circuit with two different periods at different lines (Δt = 30 ms

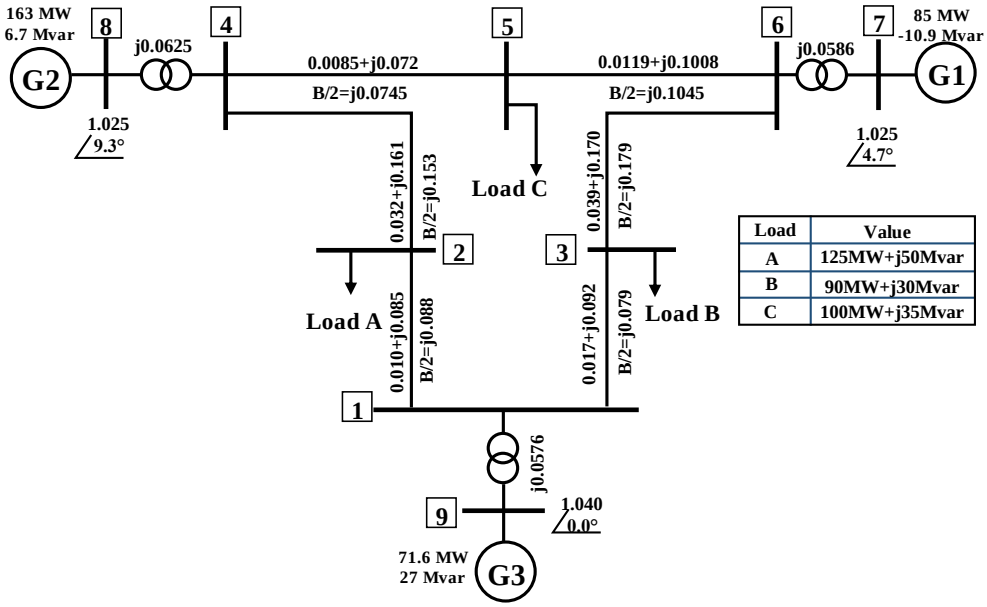

Fig. 7: The WSCC-EPS with 3-machine and 9-bus; all impedances in pu on a 100 MVA base.

and 100 ms) and the change of grid topology by elimination of a transmission line. With these different types of faults, the three DNCs are trained. After training trials, the best choice is set at seven neurons in a hidden layer for each neural network. Furthermore, performance is measured in terms of mean squared error. The evolution of these mean square learning errors $J_i (i = 1, 2, 3)$ obtained by the gradient descent algorithm is presented by Fig. 8. It is clear that the best training performance is in average 10^{-4} at epoch 200.

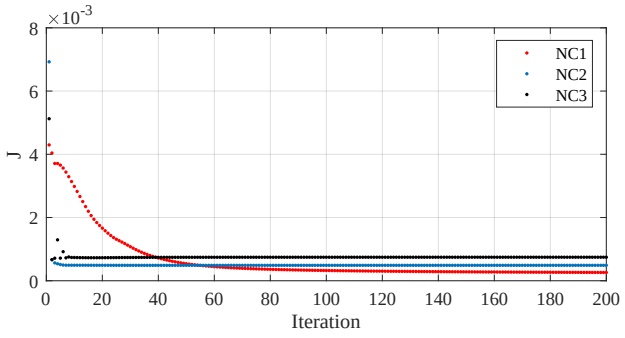

Fig. 8: Evolution of the mean square learning errors.

4.2. Simulation Results

To illustrate the results of Synthesized DNCs, a new default, not used in training process, will be applied to the EPS. The evolution of the state variables will be visualized at the time when the machine is controlled by the corresponding DNC. After the learning phase is already held, *the weights of the different neuronal networks are fixed*, which will be used to generate control laws. Indeed, simulation is performed by three sequences, which are before fault, during fault and after fault. To characterize these sequences, the steps are as follows:

Step 1: the system is in a healthy mode with an initial condition: $X_0 = [\delta_i 0\, \omega_{i0}\, E'_{qi0}]$.

Step 2: a fault is applied at t_1.

Step 3: Elimination of the fault at t_2.

Step 4: the system is in a post fault state.

In order to assess the effectiveness and robustness of the proposed DNCs, two types of faults in severe operating points of conditions are made during a simulating process: it firstly consists of step changing the load; and secondly, a three-phase short-circuit.

1) Step Change in Load A of Node 2

The applied fault to the power system is the step load changes at the consumer node 2 as addressed by: at $t_1 = 10$ s ($Pc = 2\ P_{C0}$ and $Qc = 2Q_{C0}$). Both faults were selected in such a way that they were not part of the neural network trained database. Figure 9 and Fig. 10 illustrate the outputs and the states of generator G1 and G3 respectively.

Based on Fig. 9 and according to the proposed strategy, the ϵ_s corresponding to the generator terminal voltage error, is much smaller than the one obtained by the classical controller (AVR+PSS). This criterion *highlights the high performance* of the proposed control in voltage regulation. Nevertheless, as it is presented in Fig. 10, it is possibly accentuated that the DNC gives high dynamic and static performances by compar-

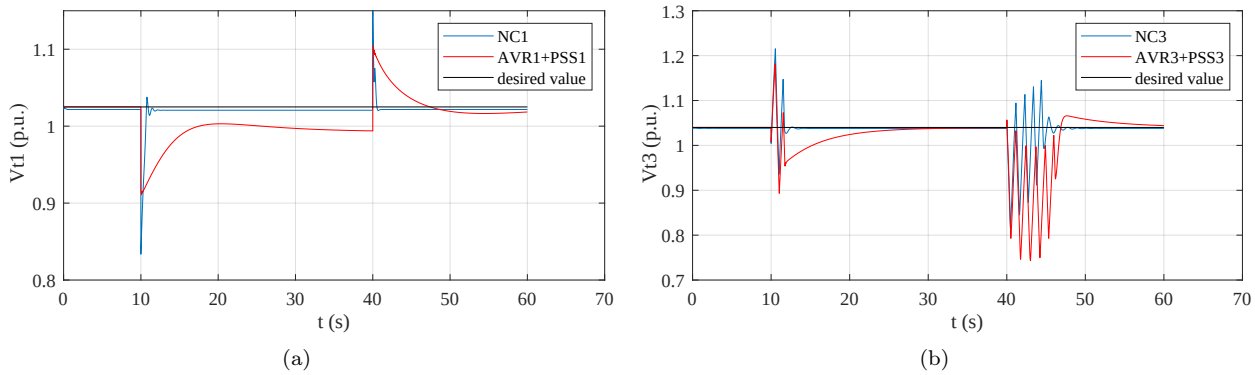

Fig. 9: Terminal voltage of the G1 (a) and G3 (b) following the step load change in Node 2.

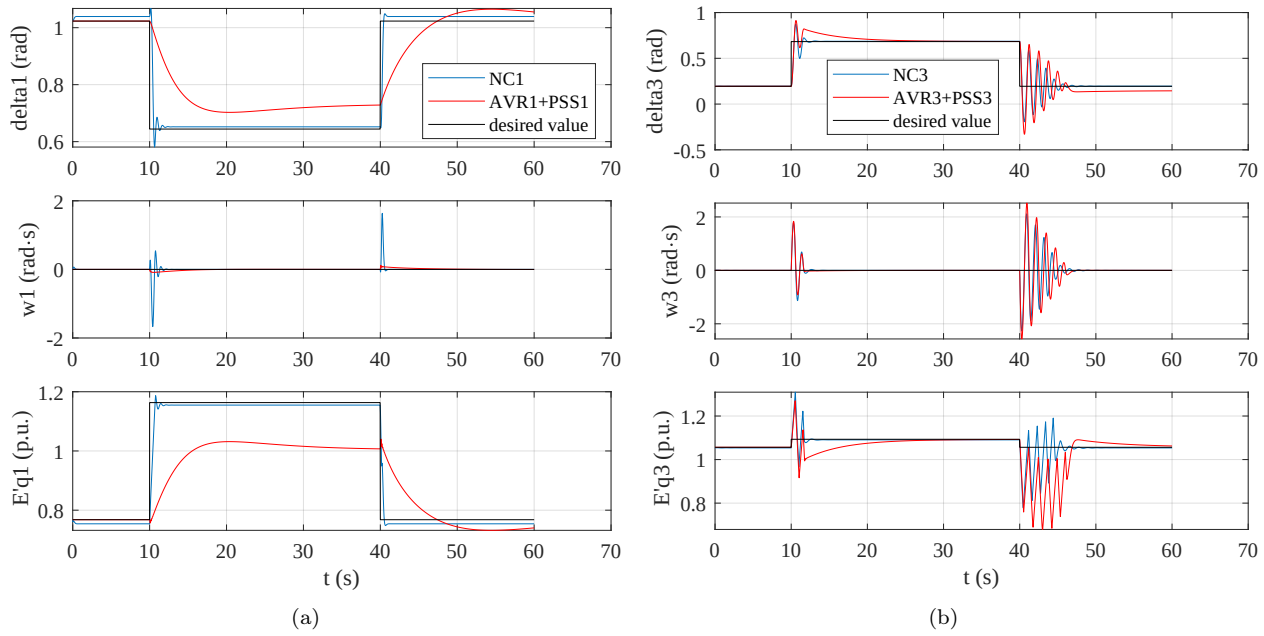

Fig. 10: State variables response of the G1 (a) and G3 (b) towards the step load change at the consumer Node 2.

ing it with the classical controller. The new controller eliminates the steady-state error for all variables (static error $\epsilon_s = 0$). Moreover, the results exhibit the DNC satisfactory performances. They show more convenient characteristics than those of the AVR+PSS control techniques, particularly those related to *the overshoot amplitude as well as the stabilizing time for* all states (δ_i, ω_i and E'_{qi}), as it is presented in Tab. 3.

Finally, the control signals evolution (excitation voltage E_{fdi}) is given in Fig. 11. It is clear to observe the use of saturation bloc (± 5 p.u.) to limit the voltage level for excitation coil protection.

2) Three Short Circuit

A three short circuit is applied to the line connecting nodes: 1 to node 2 at $t_1 = 5$ s during $\Delta t = 500$ ms. Later, the fault is eliminated by isolating the transmission line 1–2 at t_2.

With regard to Fig. 12 and Fig. 13, it is noted that by using the neural controller, the system returns to its equilibrium state after the elimination of the short circuit and the variation of its topology. However, with the classic AVR + PSS controller, the system loses its stability and basically ends up with divergence. In this respect, the improvement of the transient stability in Power Systems with Neural controller is easily noticeable with neural controller under different severe faults conditions.

Tab. 3: Overshoots and stabilizing time of G1 and G3.

Controllers	$D_1\delta$ %	$D_1\omega$ %	D'_{1E_q} %	$t_{s\delta}$ (s)	$t_{s\omega}$ (s)	t'_{sE_q} (s)
DNC1	5.5	0.2	1	1	1.5	1.5
AVR1+PSS1	2.9	0.3	2.7	13	8	15
DNC3	21	0.6	9	2	1.5	2
AVR3+PSS3	27	1.2	15	10	3	11

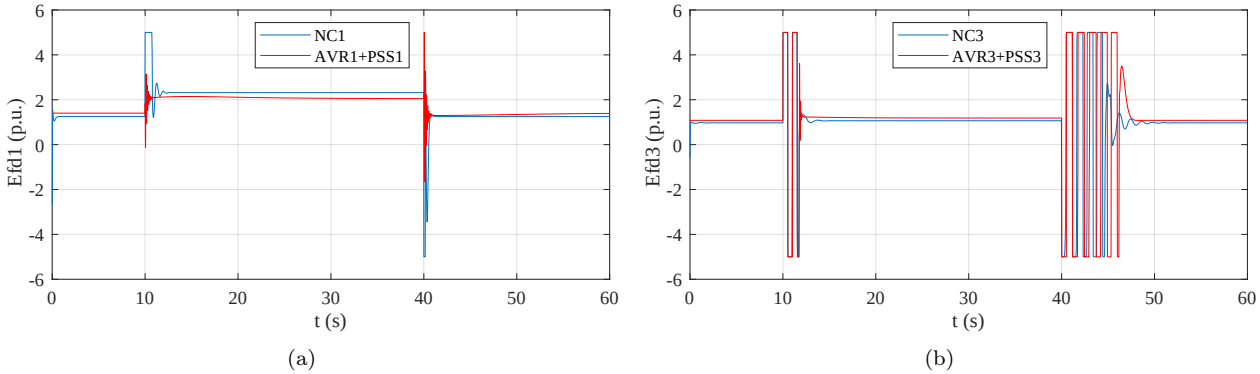

Fig. 11: Control signals evolution of G1 (E_{fd1} (p.u.)) and G3 (E_{fd3} (p.u.)) respectively.

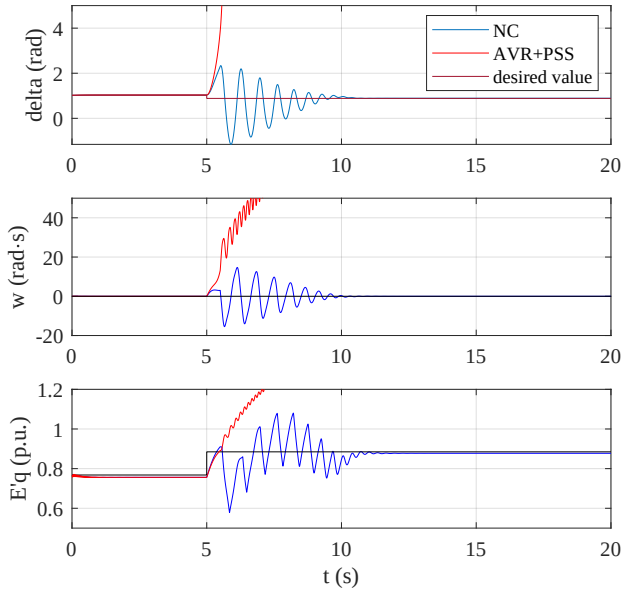

Fig. 12: The rotor angle, angular speed and the EMF of the Generator n° 1.

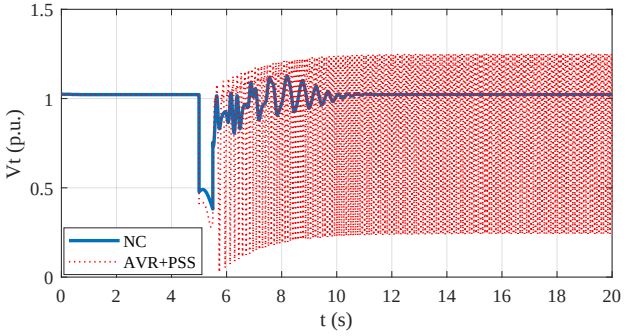

Fig. 13: Terminal voltage of the generator n° 1 V_{t1} (p.u.) during short circuit fault.

5. Conclusion

For the centralized control synthesis, the classic model is generally used in the cases the machines connected to the network are very close. Conversely, in cases they are very far away or probably the network studied is very complex, an advanced modeling approach for the synthesis of a decentralized control is suggested for the purpose of dampening the inter-zone oscillations. This advanced aggregation makes it possible to model any type of power network with the minimum number of adaptive parameters depending on the grid state. Furthermore, the possibility of training a neural network of any nonlinear function is exploited to design a nonlinear control law from a rich database for each power network generator. The advantage of this law is the stabilization of highly nonlinear systems such as the power grid even in the event of large disturbances. The proposed decentralized controller is applied to a 9-bus WSCC power system. Finally, the current findings of the synthesis of the DNCs confirm the high performances regarding the transient and dynamic stability and voltage regulation precision. Possibly for future work, the synthesized DNC will be applied for the whole EPS as a decentralized neural control strategy.

Author Contributions

W.B. developed the theoretical formalism, performed the analytic calculations and the MATLAB simulations and wrote the manuscript. Both W.B., M.B.A. and H.H authors conceived of the power system model reduction idea. M.C. encouraged W.B. to investigate a neural control for the new EPS reduced model, contributed to the final version of the manuscript and supervised the project.

References

[1] KUNDUR, P. S. *Power System Stability and Control*. 1st ed. New York: McGraw Hill, 1994. ISBN 978-0-07-035958-1.

[2] ANDERSON, P. M. and A. A. FOUAD. *Power System Control and Stability*. 2nd ed. Danvers: Wiley-IEEE Press, 2003. ISBN 978-0-470-54557-7.

[3] KAWABE, K., M. MASUDA and T. NANAHARA. Excitation control method based on wide-area measurement system for improvement of transient stability in power systems. *Electric Power Systems Research*. 2020, vol. 188, iss. 1, pp. 1–7. ISSN 0378-7796. DOI: 10.1016/j.epsr.2020.106568.

[4] ZHOU, Y., H. HUANG, Z. XU, W. HUA, F. YANG and S. LIU. Wide-area measurement system-based transient excitation boosting control to improve power system transient stability. *IET Generation, Transmission & Distribution*. 2015, vol. 9, iss. 9, pp. 845–854. ISSN 1751-8695. DOI: 10.1049/iet-gtd.2014.1030.

[5] ZHANG, S. and V. VITTAL. Design of Wide-Area Power System Damping Controllers Resilient to Communication Failures. *IEEE Transactions on Power Systems*. 2013, vol. 28, iss. 4, pp. 4292–4300. ISSN 1558-0679. DOI: 10.1109/TPWRS.2013.2261828.

[6] ALMAS, M. S., M. BAUDETTE and L. VANFRETTI. Utilizing synchrophasor-based supplementary damping control signals in conventional generator excitation systems. *Electric Power Systems Research*. 2018, vol. 157, iss. 1, pp. 157–167. ISSN 0378-7796. DOI: 10.1016/j.epsr.2017.12.004.

[7] PAUL, A., I. KAMWA and G. JOOS. Centralized Dynamic State Estimation Using a Federation of Extended Kalman Filters With Intermittent PMU Data From Generator Terminals. *IEEE Transactions on Power Systems*. 2018, vol. 33, iss. 6, pp. 6109–6119. ISSN 1558-0679. DOI: 10.1109/TPWRS.2018.2834365.

[8] WANG, C., Z. QIN, Y. HOU and J. YAN. Multi-Area Dynamic State Estimation With PMU Measurements by an Equality Constrained Extended Kalman Filter. *IEEE Transactions on Smart Grid*. 2018, vol. 9, iss. 2, pp. 900–910. ISSN 1949-3061. DOI: 10.1109/TSG.2016.2570943.

[9] LIU, H., J. SU, J. QI, N. WANG and C. LI. Decentralized Voltage and Power Control of Multi-Machine Power Systems With Global Asymptotic Stability. *IEEE Access*. 2019, vol. 7, iss. 1, pp. 14273–14282. ISSN 2169-3536. DOI: 10.1109/ACCESS.2019.2893409.

[10] CHEN, X.-B. and S. S. STANKOVIC. Overlapping decentralized approach to automation generation control of multi-area power systems. *International Journal of Control*. 2007, vol. 80, iss. 3, pp. 386–402. ISSN 1366-5820. DOI: 10.1080/00207170601001706.

[11] BIROON, R. A., P. PISU and D. SCHOENWALD. Inter-Area Oscillation Damping in Large-Scale Power Systems Using Decentralized Control. In: *ASME 2018 Dynamic Systems and Control Conference*. Atlanta: American Society of Mechanical Engineers, 2018, pp. 1–8. ISBN 978-0-7918-5190-6. DOI: 10.1115/DSCC2018-9119.

[12] SENJYU, T., Y. MORISHIMA, T. YAMASHITA, K. UEZATO and H. FUJITA. Decentralized H∞ excitation controller achieving damping of power system oscillations and terminal voltage control for multi-machine power system. In: *IEEE/PES Transmission and Distribution Conference and Exhibition*. Yokohama: IEEE, 2002, pp. 174–179. ISBN 978-0-7803-7525-3. DOI: 10.1109/TDC.2002.1178279.

[13] CUI, S., H. UKAI, H. KANDO, K. NAKAMURA and H. FUJITA. Decentralized Control of Large Power System by H∞ Control Based Excitation Control System. *IFAC Proceedings Volumes*. 1999, vol. 32, iss. 2, pp. 7370–7375. ISSN 1474-6670. DOI: 10.1016/S1474-6670(17)57257-2.

[14] CHAPMAN, J. W., M. D. ILIC, C. A. KING, L. ENG and H. KAUFMAN. Stabilizing a multimachine power system via decentralized feedback linearizing excitation control. *IEEE Transactions on Power Systems*. 1993, vol. 8, iss. 3, pp. 830–839. ISSN 0885-8950. DOI: 10.1109/59.260921.

[15] LU, Q., Y. SUN, Z. XU and T. MOCHIZUKI. Decentralized nonlinear optimal excitation control. *IEEE Transactions on Power Systems*. 1996, vol. 11, iss. 4, pp. 1957–1962. ISSN 0885-8950. DOI: 10.1109/59.544670.

[16] WANG, Y., G. GUO and D. J. HILL. Robust decentralized nonlinear controller design for multimachine power systems. *Automatica*. 1997, vol. 33, iss. 9, pp. 1725–1733. ISSN 0005-1098. DOI: 10.1016/S0005-1098(97)00091-5.

[17] LIU, H., Z. HU and Y. SONG. Lyapunov-Based Decentralized Excitation Control for Global Asymptotic Stability and Voltage Regulation of Multi-Machine Power Systems. *IEEE Transactions on Power Systems*. 2012, vol. 27, iss. 4, pp. 2262–2270. ISSN 1558-0679. DOI: 10.1109/TPWRS.2012.2196716.

[18] KENNE, G., A. M. FOMBU and J. D. D. NGUIMFACK-NDONGMO. Coordinated excitation and steam valve control for multimachine power system using high order sliding mode technique. *Electric Power Systems Research*. 2016, vol. 131, iss. 1, pp. 87–95. ISSN 0378-7796. DOI: 10.1016/j.epsr.2015.10.003.

[19] DEMIROREN, A., H. L. ZEYNELGIL and N. S. SENGOR. The application of NN technique to automatic generation control for the power system with three areas including smes units. *European Transactions on Electrical Power*. 2003, vol. 13, iss. 4, pp. 227–238. ISSN 1546-3109. DOI: 10.1002/etep.4450130404.

[20] BAHLOUL, W., R. BENAYACHE, L. CHRIFI-ALAOUI and M. B. A. KAMOUN. Combined Nonlinear Excitation Controller Dedicated to a Grid-Connected Alternator Transient Stability and Voltage Regulation Enhancement. Transactions on Systems Signals & Devices. 2010, vol. 5, iss. 2, pp. 1–18. ISSN 1861-5252

[21] SALAH, R. B., O. KAHOULI and H. HADJABDALLAH. A nonlinear Takagi-Sugeno fuzzy logic control for single machine power system. *The International Journal of Advanced Manufacturing Technology*. 2017, vol. 90, iss. 1–4, pp. 575–590. ISSN 1433-3015. DOI: 10.1007/s00170-016-9351-4.

[22] GHAHREMANI, E. and I. KAMWA. Local and Wide-Area PMU-Based Decentralized Dynamic State Estimation in Multi-Machine Power Systems. *IEEE Transactions on Power Systems*. 2016, vol. 31, iss. 1, pp. 547–562. ISSN 1558-0679. DOI: 10.1109/TPWRS.2015.2400633.

[23] PATIL, B. V., L. P. M. I. SAMPATH, A. KRISHNAN and F. Y. S. EDDY. Decentralized nonlinear model predictive control of a multimachine power system. *International Journal of Electrical Power & Energy Systems*. 2019, vol. 106, iss. 1, pp. 358–372. ISSN 0142-0615. DOI: 10.1016/j.ijepes.2018.10.018.

[24] HARDIANSYAH, S. FURUYA and J. IRISAWA. A robust H∞ power system stabilizer design using reduced-order models. *International Journal of Electrical Power & Energy Systems*. 2006, vol. 28, iss. 1, pp. 21–28. ISSN 0142-0615. DOI: 10.1016/j.ijepes.2005.09.002.

[25] HONGSHAN, Z. and L. XIAOMING. Excitation prediction control of multi-machine power systems using balanced reduced model. In: *2013 IEEE Power & Energy Society General Meeting*. Vancouver: IEEE, 2013, pp. 1–5. ISBN 978-1-4799-1303-9. DOI: 10.1109/PESMG.2013.6672420.

[26] NGUYEN, D. H. and B. WIDROW. Neural networks for self-learning control systems. *IEEE Control Systems Magazine*. 1990, vol. 10, iss. 3, pp. 18–23. ISSN 0272-1708. DOI: 10.1109/37.55119.

[27] PSALTIS, D., A. SIDERIS and A. A. YAMAMURA. A multilayered neural network controller. *IEEE Control Systems Magazine*. 1988, vol. 8, iss. 2, pp. 17–21. ISSN 0272-1708. DOI: 10.1109/37.1868.

[28] JADLOVSK, A. An Optimal Tracking Neuro-Controller for Nonlinear Dynamic Systems. *IFAC Proceedings Volumes*. 2000, vol. 33, iss. 13, pp. 483–488. ISSN 1474-6670. DOI: 10.1016/S1474-6670(17)37237-3.

[29] BEAUFAYS, F., Y. ABDEL-MAGID and B. WIDROW. Application of neural networks to load-frequency control in power systems. *Neural Networks*. 1994, vol. 7, iss. 1, pp. 183–194. ISSN 0893-6080. DOI: 10.1016/0893-6080(94)90067-1.

[30] KAMALASADAN, S., G. D. SWANN and R. YOUSEFIAN. A Novel System-Centric Intelligent Adaptive Control Architecture for Power System Stabilizer Based on Adaptive Neural Networks. *IEEE Systems Journal*. 2014, vol. 8, iss. 4, pp. 1074–1085. ISSN 1937-9234. DOI: 10.1109/JSYST.2013.2265187.

[31] VENAYAGAMOORTHY, G. K., R. G. HARLEY and D. C. WUNSCH. Dual heuristic programming excitation neurocontrol for generators in a multimachine power system. *IEEE Transactions on Industry Applications*. 2003, vol. 39, iss. 2, pp. 382–394. ISSN 0093-9994. DOI: 10.1109/TIA.2003.809438.

[32] VENAYAGAMOORTHY, G. K. and R. G. HARLEY. A continually online trained neurocontroller for excitation and turbine control of a turbogenerator. *IEEE Transactions on Energy Conversion*. 2001, vol. 16, iss. 3, pp. 261–269. ISSN 1558-0059. DOI: 10.1109/60.937206.

[33] SAERENS, M. and A. SOQUET. Neural controller based on back-propagation algorithm. *IEE Proceedings F Radar and Signal Processing*. 1991, vol. 138, iss. 1, pp. 55–62. ISSN 0956-375X. DOI: 10.1049/ip-f-2.1991.0009.

[34] PSICHOGIOS, D. C. and L. H. UNGAR. Direct and indirect model based control using artificial neural networks. *Industrial & Engineering Chemistry Research*. 1991, vol. 30, iss. 12, pp. 2564–2573. ISSN 1520-5045. DOI: 10.1021/ie00060a009.

[35] ANDERSON, P. M., T. S. YAU. Power system Dynamic Analysis Phase I, EPRI EL-0484, Projects 670-1, 1977.

About Authors

Wissem BAHLOUL received an Electrical Engineering diploma from National School of Engineering of Tunisia, Elmanar University, in 2003, his Master diploma in Electrical systems in 2004 from the same University and Ph.D. in Electrical Engineering from the National School of Engineering of Sfax, Tunisia in 2010. His research interests are focused on identification and control of Synchronous Machine, Electrical Power Systems (EPS) control and stability, and intelligent techniques applications in EPS.

Mohamed CHTOUROU received his Engineering Diploma in Electrical Engineering from the Ecole Nationale dIngenieurs de Sfax, Tunisia in 1989, D.E.A. in Automatic Control from the Institut National des Sciences Appliquees de Toulouse, France in 1990, and Ph.D. in Process Engineering from the Institut National Polytechnique of Toulouse, France in 1993 and the Habilitation Universitaire in Automatic Control from the National School of Engineering of Sfax, Tunisia in 2002. He is currently a professor in the Department of Electrical Engineering of National School of Engineers of Sfax. His current research interests include learning algorithms, artificial neural networks and their engineering applications, fuzzy systems, and intelligent control.

Mohsen BEN AMMAR received his Ph.D. in Contribution to optimizing the management of multisource renewable energy systems in Electrical Engineering from the National Engineering School of Sfax, University of Tunisia in 2011. He has been an associate professor at the University of Sfax, National Engineering School of Sfax, Tunisia. He was master technological professor at the ISET of Sfax, Tunisia, from 1998–2013. Since 2012, and a researcher in the Control and Energy Management Laboratory (CEMLab), in the National School of Engineers of Sfax, Tunisia. His current research interests are Electrical Power System (EPS) and renewable energies management, monitoring system, fuzzy logic and genetic algorithms.

Hsan HADJ ABDALAH received his M.Sc. in electrical engineering from the superior normal school of Technical teaching of Tunis-Tunisia in 1982, the Diplome d'Etudes Aprofondies in electrical engineering from the superior normal school of Technical teaching of Tunis-Tunisia in 1991 and habilitation universitaire in electrical engineering from the Diploma in electrical engineering from the National School of Engineers of Sfax, Tunisia in 2007. He is currently an associate professor in the department of Electrical Engineering of National School of Engineers of Sfax-Tunisia. His current research interests include electrical power systems, the dispatching and the stability of EPS, wind energy, and intelligent techniques applications in EPS.